Robust Model-based H_∞ control for Free-floating Space Manipulator Cartesian Motions*

Dimitrios Anastasiou, Kostas Nanos, and Evangelos Papadopoulos, *Fellow, IEEE*

Abstract. During on-orbit tasks, when space manipulator systems (SMS) need to handle captured unknown objects accurately, robust control for compensation of uncertainties and disturbances is required. To avoid fuel consumption and/or sudden end-effector impacts with the object, the SMS is in free-floating mode, i.e., the base is not actuated. In this work, a robust Cartesian-space controller is developed for a free-floating SMS during object capture. The controller consists of a model-based part, which linearizes the dynamics globally and guarantees specific performance, and of a linear H_∞ part, that assists by adding robustness in the presence of parametric uncertainties and/or disturbances. It is shown that the developed controller minimizes tracking errors and attenuates sensor noise. The sensitivity of the developed controller to uncertainties is studied by Monte Carlo simulations; the resulting tracking errors are an order of magnitude smaller than those obtained without H_∞ compensation. The control method applies to spatial systems and is demonstrated by a planar example.

I. Introduction

In space applications, such as on-orbit assembly, maintenance, repair, refueling, and deorbiting of space debris, robustness in the control algorithms employed has been of significant concern [1]. In the coming years, on-orbit space manipulator systems (SMS) will play a significant role in a wide variety of space operations. A SMS includes a spacecraft (S/C) equipped with one or more robotic manipulators, see Fig. 1. The position and attitude of the S/C is controlled by the Attitude Determination and Control System (ADCS). The end-effector position and orientation are set by joint motors controlled by the manipulator control system [2]. For safety reasons, each of these control systems operates independently; however, due to dynamic coupling, the manipulator motion affects the motion of the S/C and vice versa. To avoid undesirable and perhaps sudden disturbances to the end-effector motion, it is preferable to have the ADCS turned-off. Then, the system operates in a free-floating mode, in which both thruster fuel and control momentum device electrical power are not consumed, extending system life.

To accomplish tasks accurately and avoid dangerous impacts, advanced model-based control strategies, which require accurate knowledge of system parameters, are necessary [3]. However, the dynamic properties of a SMS may change on orbit for several reasons, such as fuel consumption, deployment of payload, or capture of an unknown object. One way to tackle this issue is to design adaptive control laws whose parameters are adapted to obtain the desired system response despite the inaccurate knowledge of its parameters, [4]. However, even though adaptive control laws have been proposed for free-flying SMS (i.e., active ADCS), [5], there are strong limitations to their application on under-actuated free-floating SMS (FFSMS), [6].

Another approach to address uncertainties in the feedback system, is to employ robust controllers such as a Sliding Mode Control (SMC), [4] or the H_∞ control methodology [7]. The SMC can be applied to nonlinear systems such as the SMS. However chattering, and excessive control effort restrict its application, [8]. The H_∞ methodology has been applied to a variety of applications, such as the control of large space structures [9] or of satellites with large solar arrays or antennas [10]. However, these systems are approximately linear and are treated as such. The design of an H_∞ controller was proposed to tackle the nanosatellite rendezvous and docking problem, also considering the fuel sloshing effect [11].

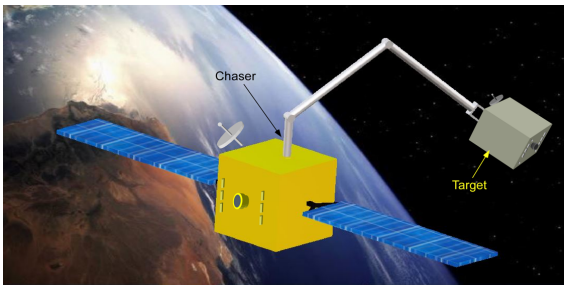

Fig. 1. A space manipulator system (chaser) capturing space object (target).

The problem of tracking control of guaranteed performance for FFSMS with plant uncertainties and external disturbances, was studied using an adaptive nonlinear H_∞ controller via neural networks [12]. Recently, non-linear H_∞ controllers have been proposed for a SMS operating in a controlled – floating mode where both the S/C attitude and manipulator joints are controlled, [13] – [15]. However, the design of a nonlinear H_∞ is more complex than the design of a linear one since the design variables are not directly related

* Kostas Nanos' research is co-financed by the Greece and European Union (European Social Fund-ESF) through the Operational Programme «Human Resources Development, Education and Lifelong Learning» in the context of the project "Reinforcement of Postdoctoral Researchers - 2nd Cycle" (MIS-5033021), implemented by the State Scholarships Foundation (IKY).

Dimitrios Anastasiou is with the WEISS, UCL, e-mail: dimitrios.anastasiou.21@ucl.ac.uk. This work was done while at NTUA.

Kostas Nanos & Evangelos Papadopoulos are with the School of Mechanical Engineering, National Technical University of Athens, Greece (e-mail: nanos.kostas@gmail.com, egpapado@central.ntua.gr.

to system performance. This leads to high forces/ torques and a degradation of system performance. On the other hand, linear H_∞ controllers generally offer transparency and interpretability, essential requirements for space missions.

Although in space applications, H_∞ controllers for locally linearized systems (e.g., satellites) have been studied thoroughly, for example see [9] - [11], these are not suitable for strongly non-linear and configuration dependent SMS. To accomplish tasks in joint space, the design of a linear H_∞ controller has been tested on a dynamically equivalent dual-arm manipulator [16]; however, the ability of the scheme to compensate for parametric uncertainties and sensor noise was not tested, while the full potential of the linear H_∞ framework with respect to disturbances and control effort has not been exploited. Hence, the design of H_∞ controllers for SMS with parametric uncertainty, subject to disturbances, while performing tasks in Cartesian space, remains unaddressed.

In this paper, the post-capture, Cartesian space motion control of an unknown object by a parametrically uncertain FFSMS is studied. The proposed methodology allows the control of an inherently non-linear system with parametric uncertainty and subject to unknown disturbances. The developed controller consists of two feedback loops. The first is a model-based algorithm, which linearizes the dynamics globally and guarantees specific performance. This is assisted by a linear H_∞ law, that adds robustness to the end-effector response. It is shown that the developed controller minimizes tracking errors and attenuates sensor noise. The sensitivity of the developed controller to uncertainties is studied by Monte Carlo simulations; it is found that the resulting tracking errors are an order of magnitude smaller than those obtained without H_∞ compensation. The control method applies to spatial systems and is demonstrated by a planar example.

II. Dynamics of Free-Floating Space Manipulators

In this section, the dynamics of a spatial FFSMS with a N degree-of-freedom (dof) manipulator is briefly described. In the absence of external torques, the system angular momentum is conserved. The design of the proposed controller is not affected by the existence of small amounts of non-zero angular momentum. Therefore, without loss of generality, it is assumed that the initial angular momentum of the system is zero. In this case, the conservation equation is, [3]

$$\mathbf{R}_0(\boldsymbol{\varepsilon},n)\left[{}^0\mathbf{D}(\mathbf{q})\,{}^0\boldsymbol{\omega}_0+{}^0\mathbf{D}_\mathbf{q}(\mathbf{q})\dot{\mathbf{q}}\right]=\mathbf{0}_{3x1} \tag{1}$$

where ${}^0\boldsymbol{\omega}_0$ is the S/C angular velocity expressed in the S/C frame, the $N\times1$ column vectors $\mathbf{q},\dot{\mathbf{q}}$ represent manipulator relative joint angles and rates respectively, ${}^0\mathbf{D}(\mathbf{q})$, ${}^0\mathbf{D}_\mathbf{q}(\mathbf{q})$ are inertia-type matrices of appropriate dimensions, see [3], and $\mathbf{0}_{kxm}$ is the $k\times m$ zero matrix. $\mathbf{R}_0(\boldsymbol{\varepsilon},n)$ is the rotation matrix between the S/C frame and the inertial frame expressed as a function of the S/C Euler parameters (unit quaternions) $\boldsymbol{\varepsilon},n$.

The end-effector linear velocity $\dot{\mathbf{r}}_\mathbf{E}$ and angular velocity $\boldsymbol{\omega}_\mathbf{E}$ are given by, [3]

$$\begin{bmatrix}\dot{\mathbf{r}}_\mathbf{E}\\ \boldsymbol{\omega}_\mathbf{E}\end{bmatrix}=\mathbf{R}_0^*(\boldsymbol{\varepsilon},n)\,{}^0\mathbf{J}_\mathbf{q}(\mathbf{q})\dot{\mathbf{q}} \tag{2}$$

where

$$\mathbf{R}_0^*(\boldsymbol{\varepsilon},n)=\begin{bmatrix}\mathbf{R}_0(\boldsymbol{\varepsilon},n) & \mathbf{0}_{3x3}\\ \mathbf{0}_{3x3} & \mathbf{R}_0(\boldsymbol{\varepsilon},n)\end{bmatrix} \tag{3}$$

and the $6\times N$ matrix ${}^0\mathbf{J}_\mathbf{q}(\mathbf{q})$ is the Generalized Jacobian Matrix expressed in the S/C frame. This matrix is a function of the manipulator configuration $\mathbf{q}$ and is given by:

$${}^0\mathbf{J}_\mathbf{q}(\mathbf{q})=\begin{bmatrix}{}^0\mathbf{J}_{12}(\mathbf{q})-{}^0\mathbf{J}_{11}(\mathbf{q})\,{}^0\mathbf{D}^{-1}(\mathbf{q})\,{}^0\mathbf{D}_\mathbf{q}(\mathbf{q})\\ {}^0\mathbf{J}_{22}(\mathbf{q})-{}^0\mathbf{D}^{-1}(\mathbf{q})\,{}^0\mathbf{D}_\mathbf{q}(\mathbf{q})\end{bmatrix} \tag{4}$$

where the terms ${}^0\mathbf{J}_{11}(\mathbf{q}),{}^0\mathbf{J}_{12}(\mathbf{q}),{}^0\mathbf{J}_{22}(\mathbf{q})$ are Jacobian-type matrices of appropriate dimensions.

In case the end-effector attitude is expressed as a function of Euler angles $\boldsymbol{\theta}_\mathbf{E}$, the following equation can be used

$$\boldsymbol{\omega}_\mathbf{E}=\mathbf{E}(\boldsymbol{\theta}_\mathbf{E})\dot{\boldsymbol{\theta}}_\mathbf{E} \tag{5}$$

where $\mathbf{E}(\boldsymbol{\theta}_\mathbf{E})$ is a 3×3 matrix. Then, the end-effector velocity is expressed as,

$$\mathbf{v}_\mathbf{E}=\begin{bmatrix}\dot{\mathbf{r}}_\mathbf{E}\\ \dot{\boldsymbol{\theta}}_\mathbf{E}\end{bmatrix}=\mathbf{J}_\mathbf{q}^*(\mathbf{q},\boldsymbol{\theta}_\mathbf{E})\dot{\mathbf{q}} \tag{6}$$

where

$$\mathbf{J}_\mathbf{q}^*(\mathbf{q},\boldsymbol{\theta}_\mathbf{E},\boldsymbol{\varepsilon},n)=\begin{bmatrix}\mathbf{I}_3 & \mathbf{0}_{3x3}\\ \mathbf{0}_{3x3} & \mathbf{E}^{-1}(\boldsymbol{\theta}_\mathbf{E})\end{bmatrix}\mathbf{R}_0^*(\boldsymbol{\varepsilon},n)\,{}^0\mathbf{J}_\mathbf{q}(\mathbf{q}) \tag{7}$$

where $\mathbf{I}_\mathbf{k}$ is the $k\times k$ unity matrix.

With zero angular momentum and negligible gravitational forces and other external disturbances, the reduced equations of motion of the spatial FFSMS in the *joint* space are, [3]

$$\mathbf{H}_\mathbf{q}(\mathbf{q})\ddot{\mathbf{q}}+\mathbf{C}_\mathbf{q}(\mathbf{q},\dot{\mathbf{q}})\dot{\mathbf{q}}=\boldsymbol{\tau} \tag{8}$$

where $\boldsymbol{\tau}$ is the $N\times1$ column-vector of the manipulator joint torques. The *reduced* system inertia matrix $\mathbf{H}_\mathbf{q}(\mathbf{q})$ is given by, [3]

$$\mathbf{H}_\mathbf{q}(\mathbf{q})={}^0\mathbf{D}_{\mathbf{qq}}-{}^0\mathbf{D}_\mathbf{q}^\mathrm{T}\,{}^0\mathbf{D}^{-1}\,{}^0\mathbf{D}_\mathbf{q} \tag{9}$$

The matrix $\mathbf{C}_\mathbf{q}(\mathbf{q},\dot{\mathbf{q}})$ containing nonlinear Coriolis and centrifugal terms is given by, [3]

$$\begin{aligned}\mathbf{C}_\mathbf{q}(\mathbf{q},\dot{\mathbf{q}})=&\frac{1}{2}\frac{\partial(\dot{\mathbf{q}}^\mathrm{T}\,{}^0\mathbf{D}_\mathbf{q}^\mathrm{T}\,{}^0\mathbf{D}^{-1}\,{}^0\mathbf{D}_\mathbf{q})}{\partial\mathbf{q}}+\frac{\partial({}^0\mathbf{D}_{\mathbf{qq}}\dot{\mathbf{q}})}{\partial\mathbf{q}}\\ &-\frac{1}{2}\frac{\partial(\dot{\mathbf{q}}^\mathrm{T}\,{}^0\mathbf{D}_{\mathbf{qq}})}{\partial\mathbf{q}}-\frac{\partial({}^0\mathbf{D}_\mathbf{q}^\mathrm{T}\,{}^0\mathbf{D}^{-1}\,{}^0\mathbf{D}_\mathbf{q}\dot{\mathbf{q}})}{\partial\mathbf{q}}\end{aligned} \tag{10}$$

where the matrix ${}^0\mathbf{D}_{\mathbf{qq}}$ is an inertia-type matrix, see [3].

The equations of motion in the joint space, given by (8), are transformed to the *Cartesian* space. Differentiating (6), the end-effector linear and angular acceleration are given by

$$\dot{\mathbf{v}}_\mathbf{E}=\mathbf{J}_\mathbf{q}^*(\mathbf{q},\boldsymbol{\theta}_\mathbf{E},\boldsymbol{\varepsilon},n)\ddot{\mathbf{q}}+\dot{\mathbf{J}}_\mathbf{q}^*(\mathbf{q},\boldsymbol{\theta}_\mathbf{E},\boldsymbol{\varepsilon},n,\dot{\mathbf{q}},\dot{\boldsymbol{\theta}}_\mathbf{E},\dot{\boldsymbol{\varepsilon}},\dot{n})\dot{\mathbf{q}} \tag{11}$$

Assuming that the Jacobian matrix $\mathbf{J}_\mathbf{q}^*$ is invertible, (11) can be solved for the joint accelerations:

$$\ddot{\mathbf{q}}=\mathbf{J}_\mathbf{q}^{*-1}\dot{\mathbf{v}}_\mathbf{E}-\mathbf{J}_\mathbf{q}^{*-1}\dot{\mathbf{J}}_\mathbf{q}^*\dot{\mathbf{q}} \tag{12}$$

Note that, depending on the desired end-effector Cartesian

path, one can always find an appropriate FFSMS initial configuration to guarantee that the matrix $\mathbf{J}_q^*$ is always invertible during the end-effector motion, [17].

The substitution of (12) in (8), results in the equations of motion in the Cartesian space:

$$\mathbf{H}_x \dot{\mathbf{v}}_E + \mathbf{c}_x = \mathbf{u} \tag{13}$$

where

$$\mathbf{u} = \mathbf{J}_q^{*-T} \boldsymbol{\tau} \tag{14}$$

$$\mathbf{H}_x = \mathbf{J}_q^{*-T} \mathbf{H}_q \mathbf{J}_q^{*-1} \tag{15}$$

$$\mathbf{c}_x = \mathbf{J}_q^{*-T} (\mathbf{C}_q - \mathbf{H}_q \mathbf{J}_q^{*-1} \dot{\mathbf{J}}_q^*) \mathbf{J}_q^{*-1} \mathbf{v}_E \tag{16}$$

The FFSMS dynamics in Cartesian space are employed next in the design of the developed model-based control law.

III. Controller Design

A. Controller Structure

The developed controller linearizes and decouples the nonlinear and coupled dynamics of the FFSMS using a model-based controller; the uncertainty is compensated by a linear H_∞ control law. Therefore, the controller scheme consists of two feedback loops, one formed by the model-based and the other formed by the H_∞.

The controller structure is shown in Fig. 2. The control input is given by,

$$\mathbf{u} = \hat{\mathbf{H}}_x \dot{\mathbf{v}}_E^* + \hat{\mathbf{c}}_x - \hat{\mathbf{H}}_x \mathbf{u}_\infty \tag{17}$$

where $(\hat{\cdot})$ denotes nominal value of $(\cdot)$, the $N \times 1$ column vector $\mathbf{u}_\infty$ is the H_∞ law contribution to the controller and

$$\dot{\mathbf{v}}_E^* = \dot{\mathbf{v}}_{E,d} + \mathbf{K}_v \dot{\mathbf{e}}_x + \mathbf{K}_p \mathbf{e}_x \tag{18}$$

where $\dot{\mathbf{v}}_{E,d}$ is the desired linear and angular end-effector acceleration and $\mathbf{e}_x$ is the tracking error defined by

$$\mathbf{e}_x = \begin{bmatrix} \mathbf{r}_{E,d} - \mathbf{r}_E \\ \boldsymbol{\theta}_{E,d} - \boldsymbol{\theta}_E \end{bmatrix} \tag{19}$$

where $(\cdot)_d$ denotes the desired value of variable $(\cdot)$.

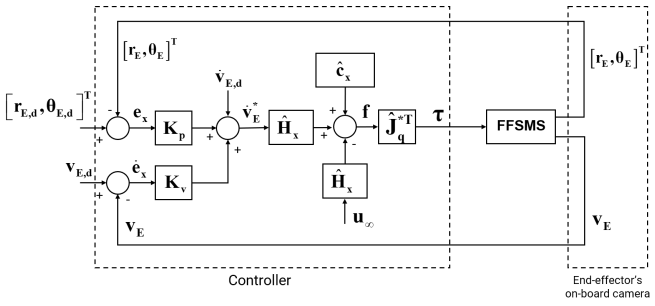

Fig. 2. Controller structure. The H_∞ controller contributes through $\mathbf{u}_\infty$.

The $N \times N$ gain matrices $\mathbf{K}_p$ and $\mathbf{K}_v$ are chosen as,

$$\mathbf{K}_p = diag(\omega_{n_1}^2, \cdots, \omega_{n_N}^2), \mathbf{K}_v = diag(2\zeta\omega_{n_1}, \cdots, 2\zeta\omega_{n_N}) \tag{20}$$

where the damping ration ζ and the natural frequency ω_{n_i} correspond to the closed-loop system desired response.

Considering (14), the required joint torques are,

$$\boldsymbol{\tau} = \hat{\mathbf{J}}_q^{*T} \mathbf{u} \tag{21}$$

Combining (13) with (17) – (18) results in the following error dynamics of the closed – loop system,

$$\ddot{\mathbf{e}}_x + \mathbf{K}_v \dot{\mathbf{e}}_x + \mathbf{K}_p \mathbf{e}_x = \mathbf{u}_\infty + \mathbf{d}_{unc} \tag{22}$$

where,

$$\mathbf{d}_{unc} = \hat{\mathbf{H}}_x^{-1} \left[(\mathbf{H}_x - \hat{\mathbf{H}}_x) \dot{\mathbf{v}}_E + (\mathbf{c}_x - \hat{\mathbf{c}}_x) \right] \tag{23}$$

is a term due to the parametric uncertainty and acts as a disturbance to the closed loop system formed by the model-based controller. It is desired that the right-hand side of (22) is zero. This is feasible if $\mathbf{u}_\infty$ cancels $\mathbf{d}_{unc}$ for all time.

B. Design of the linear H_∞ control law

To design a linear H_∞ control law, the term $\mathbf{d}_{unc}$ is temporarily ignored and (22) is written as,

$$\ddot{\mathbf{e}}_x + \mathbf{K}_v \dot{\mathbf{e}}_x + \mathbf{K}_p \mathbf{e}_x = \mathbf{u}_\infty \tag{24}$$

In this case, the representation of (24) in state-space is,

$$\dot{\mathbf{e}} = \mathbf{A}\mathbf{e} + \mathbf{B}\mathbf{u}_\infty \tag{25}$$

$$\mathbf{y} = \mathbf{e} = \mathbf{C}\mathbf{e} + \mathbf{D}\mathbf{u}_\infty \tag{26}$$

where

$$\mathbf{A} = \begin{bmatrix} \mathbf{0}_{N\times N} & \mathbf{I}_N \\ -\mathbf{K}_p & -\mathbf{K}_v \end{bmatrix}, \quad \mathbf{B} = \begin{bmatrix} \mathbf{0}_{N\times N} \\ \mathbf{I}_N \end{bmatrix}$$
$$\mathbf{C} = \begin{bmatrix} \mathbf{I}_N & \mathbf{0}_{N\times N} \\ \mathbf{0}_{N\times N} & \mathbf{I}_N \end{bmatrix}, \quad \mathbf{D} = \begin{bmatrix} \mathbf{0}_{N\times N} \\ \mathbf{0}_{N\times N} \end{bmatrix} \tag{27}$$

and

$$\mathbf{e} = \begin{bmatrix} \mathbf{e}_x \\ \dot{\mathbf{e}}_x \end{bmatrix} \tag{28}$$

Note, that the H_∞ methodology is valid for rational and proper systems. By selecting appropriate gains $\mathbf{K}_p$, and $\mathbf{K}_v$ in (24), these requirements are satisfied.

Next, a Generalized Block Diagram (GBD) is created as shown in Fig. 3. The $p \times m$ transfer matrix $\mathbf{G}(s)$ results from (25) – (26) and the $m \times p$ matrix $\mathbf{K}(s)$ is the control law where $m = N$ is the number of system inputs and $p = 2N$ is the number of system outputs.

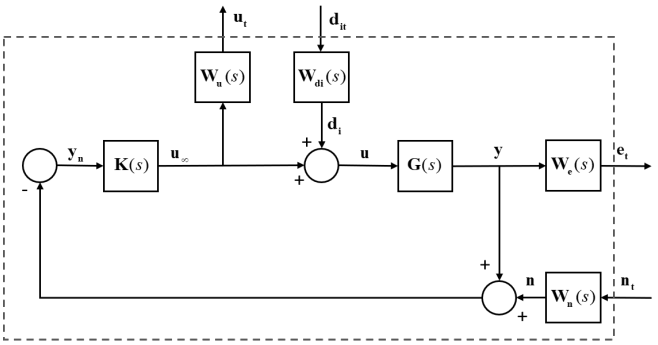

Fig. 3. Generalized Block Diagram.

The signals that enter the dashed box of the GBD, see Fig. 3, are the outside influences, and those exiting it are the regulated variables. The $(m+p) \times 1$ column vectors of the outside influences and regulated variables, are defined respectively, as,

$$\mathbf{w} = \begin{bmatrix} \mathbf{d}_{it} \\ \mathbf{n}_t \end{bmatrix}, \quad \mathbf{z} = \begin{bmatrix} \mathbf{e}_t \\ \mathbf{u}_t \end{bmatrix} \tag{29}$$

The $m \times m$ matrices $\mathbf{W}_u(s), \mathbf{W}_{di}(s)$ and the $p \times p$ matrices $\mathbf{W}_e(s), \mathbf{W}_n(s)$ are weighting functions and

controller design variables, with their own objective. $\mathbf{W_u}(s)$ is used to reduce the control effort $\mathbf{u}_\infty$, $\mathbf{W_{di}}(s)$ is used to model the type of disturbances $\mathbf{d_i}$ expected at system input, $\mathbf{W_e}(s)$ is used to shape system performance, and $\mathbf{W_n}(s)$ is used to model the expected sensor noise $\mathbf{n}$. Established guidelines indicate that these matrices may have the form [7]

$$\mathbf{W_e}(s)=\left(\frac{s/\sqrt[k]{M_s}+\omega_b}{s+\omega_b\sqrt[k]{\varepsilon}}\right)^k\cdot\mathbf{I_{2N}},\ k\geq 1 \tag{30}$$

$$\mathbf{W_u}(s)=\left(\frac{s+\omega_{bc}/\sqrt[k]{M_u}}{\sqrt[k]{\varepsilon_1}s+\omega_{bc}}\right)^k\cdot\mathbf{I_N},\ k\geq 1 \tag{31}$$

where $M_s=\|\mathbf{S}\|_\infty$ is the maximum of the Sensitivity Function $\mathbf{S}$, ω_b is the desired closed-loop bandwidth, ε is the desired steady state error with respect to a step input, M_u is the maximum gain measured by $\|\mathbf{KS}\|_\infty$, ω_{bc} is the controller's bandwidth, ε_1 is a small real number, k is a positive integer that determines the roll-off rate of the closed – loop system and $\|(\cdot)\|_\infty$ indicates the H_∞ norm of $(\cdot)$.

Typically, the weighting functions $\mathbf{W_{di}}(s)$ and $\mathbf{W_n}(s)$ are diagonal matrices, with their diagonal elements represented by low-pass and high-pass filters respectively.

To design an H_∞ law, the weighting functions must be selected carefully to yield the $\mathbf{K}(s)$ that minimizes the effect of the outside influences to the regulated variables. Therefore, this is a minimization problem with cost function $\|\mathbf{T_{zw}}\|_\infty$, where $\mathbf{T_{zw}}$ is the lower Linear Fractional Transformation (LFT) of the Augmented Plant $\mathbf{M}$ and $\mathbf{K}$ denoted by $\mathbf{T_{zw}}=F_l(\mathbf{M},\mathbf{K})$. The GBD can now be transformed into the LFT framework, see Fig. 4.

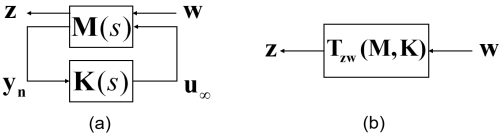

Fig. 4. Controller scheme concept.

From Fig. 4(a) one can observe that

$$\begin{bmatrix}\mathbf{z}\\ \mathbf{y_n}\end{bmatrix}=\mathbf{M}(s)\begin{bmatrix}\mathbf{w}\\ \mathbf{u}_\infty\end{bmatrix}\Rightarrow\begin{bmatrix}\mathbf{e_t}\\ \mathbf{u_t}\\ \mathbf{y_n}\end{bmatrix}=\mathbf{M}(s)\begin{bmatrix}\mathbf{d_{it}}\\ \mathbf{n_t}\\ \mathbf{u}_\infty\end{bmatrix} \tag{32}$$

Considering the GBD in Fig. 3, the matrix $\mathbf{M}(s)$ in (32) is

$$\mathbf{M}(s)=\begin{bmatrix}\mathbf{W_eGW_{di}} & \mathbf{0}_{p\times p} & \mathbf{W_eG}\\ \mathbf{0}_{m\times m} & \mathbf{0}_{m\times p} & \mathbf{W_u}\\ \mathbf{-GW_{di}} & \mathbf{-W_n} & \mathbf{-G}\end{bmatrix} \tag{33}$$

As mentioned above, the design of a linear H_∞ controller requires the selection of appropriate weighting functions. However, the selection of these functions is not trivial, since each has its own goal, and in many cases these goals are in conflict. Moreover, the design of these functions is done in the frequency domain, while in many cases the design requirements are given in the time domain (e.g., small tracking errors). The final selection of the appropriate weighting functions is achieved by a trade-off analysis.

Considering the standard assumptions for matrix $\mathbf{M}(s)$ and performing an iterative algorithm which involves the solution of two Riccati equations [7], one can find the controller $\mathbf{K}(s)$, which eventually leads to the feedback law

$$\mathbf{u}_\infty=-\mathbf{K}(s)\mathbf{e} \tag{34}$$

The order of the law $\mathbf{K}(s)$ is usually much larger than the system order, making the application of H_∞ impractical. To tackle this limitation, the order of $\mathbf{K}(s)$ is reduced using the Hankel Singular Values [7].

The controller feedback includes the relative joint angles, and the S/C attitude and angular velocity, which can be measured using appropriate sensors such as encoders, on-board star, and sun sensors, and IMUs. Other variables are computed based on them.

C. Controller Design Evaluation

The effectiveness of the linear H_∞ law design is evaluated by the value of the parameter γ, defined by, $\gamma=\|\mathbf{T_{zw}}\|_\infty$. Some guidelines suggest that $\gamma<1.8$. Obviously, this is not enough by itself; however, very large values of γ indicate poor controller design.

The stability and performance with respect to time domain specifications, such as disturbance and noise attenuation, and parametric uncertainty, determine a design's success. The stability of the closed loop system can be studied by computing the H_∞ norm of the sensitivity function $\|\mathbf{S}\|_\infty$, which must be relatively small, and the system Gain Margin (GM) and Phase Margin (PM), using the following criteria

$$GM\geq\|\mathbf{S}\|_\infty\cdot\left(\|\mathbf{S}\|_\infty-1\right)^{-1},\ PM\geq 2\arcsin\left(2\|\mathbf{S}\|_\infty\right)^{-1} \tag{35}$$

Typical values for these margins are

$$GM\geq 6dB\ ,\quad PM\geq 30\deg \tag{36}$$

To evaluate closed-loop system performance, one should examine the singular values of the sensitivity function $\mathbf{S}$, the loop gain function $\mathbf{L}$ and the complementary sensitivity function $\mathbf{T}$, as they must have specific shapes. Additionally, the norms $\|\mathbf{W_eS}\|_\infty$, and $\|\mathbf{W_uKS}\|_\infty$ must be small.

Next, the control design is evaluated with an example.

IV. Example & Results

In this example, the developed controller is studied and validated via simulations on Simulink and ADAMS, see Fig. 5(a), for tasks in which on-orbit assembly of large structures is performed using a FFSMS.

Without loss of generality, the planar three link FFSMS (N=3) shown in Fig. 5(b) with nominal parameters presented in Table I, is studied. The nominal parameters of the target are shown in Table II.

The FFSMS is required to move an uncertain target body accurately, therefore a robust controller is needed. To avoid undesirable collisions during the motion, the end-effector is commanded to follow a desired Cartesian trajectory.

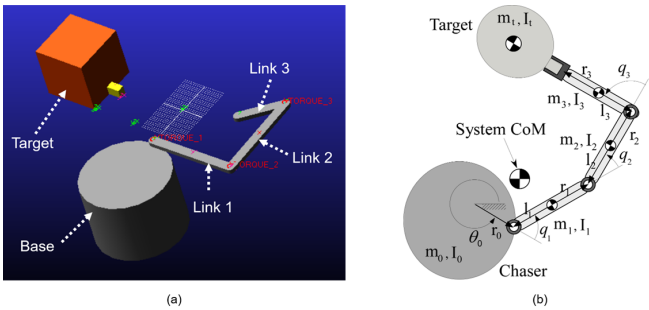

(a) (b)

Fig. 5. (a) The chaser and target models in ADAMS and (b) the definition of system parameters.

TABLE I. NOMINAL PARAMETERS FOR THE FFSMS SHOWN IN FIG. 5.

Body	$\hat{m}_i$ (kg)	$\hat{r}_i$ (m)	$\hat{l}_i$ (m)	$\hat{I}_i$ (kg m^2)
0	2000	1.5	-	2250
1	50	1.0	1.0	16.66
2	50	1.0	1.0	16.66
3	20	0.5	0.5	1.66

TABLE II. NOMINAL PARAMETERS OF THE TARGET SHOWN IN FIG. 5.

Body	$\hat{m}_t$ (kg)	$\hat{I}_t$ (kg m^2)
t	200	25

Due to the captured target, the third link total mass now is:

$$m_3' = m_3 + m_t \tag{37}$$

Also, the third link's center of mass (CoM), defined by the vectors $\hat{r}_3$ and $\hat{l}_3$, and its polar moment of inertia $\hat{I}_3$ respectively have changed to

$$l_3' = \left(m_3 l_3 + m_t (l_3 + r_3)\right) / m_3' \tag{38}$$

$$r_3' = r_3 + l_3 - l_3' \tag{39}$$

$$I_3' = I_3 + m_3 (l_3' - l_3)^2 + m_t r_3'^2 \tag{40}$$

Here, the uncertainty in the target mass is assumed to be,

$$0.75\hat{m}_t \le m_t \le 1.25\hat{m}_t \tag{41}$$

Also, the uncertainty on the SMS's S/C mass due to fuel consumption during orbital maneuvers is considered. Assuming an uncertainty of $40kg$ in fuel consumption, the uncertainty in S/C total mass is,

$$1960kg \le m_0 \le 2040kg \tag{42}$$

To deal with both the target and S/C parametric uncertainties given by (41) - (42), the developed model-based plus H_∞ controller is employed. To achieve a critically damped performance of the closed-loop system with settling time $t_s = 3s$, (i.e., $\zeta = 1$ and $\omega_n = 2 rad/s$), the model-based controller gains, are selected using (20) as,

$$\mathbf{K_p} = diag(4,4,4), \quad \mathbf{K_v} diag(4,4,4) \tag{43}$$

The weighting functions are selected by methodologies proposed in [18], as

$$\mathbf{W_e}(s) = \frac{s+1}{0.5s+0.1} \cdot \mathbf{I_6}, \quad \mathbf{W_u}(s) = \left(\frac{s+5}{s+50}\right)^2 \cdot \mathbf{I_3}$$
$$\mathbf{W_{di}}(s) = \mathbf{I_3}, \qquad \mathbf{W_n}(s) = 0.01\frac{s+10}{s+100} \cdot \mathbf{I_6} \tag{44}$$

Using these weighting functions as inputs in Matlab function "*hinfsyn*" and function "*reduce*" to reduce the controller order from 24 to 6, the following are obtained,

$$\gamma = 0.121, \ \|S\|_\infty = 1.92, \ GM = 6.35dB, \ PM = 30.07 \deg \tag{45}$$

Note that the controller design does not depend on the selected end-effector desired trajectory. In capture operations, the end-effector desired trajectories are usually short and slow. Here, the end-effector is commanded to move from point (1.7, 1.2) to point (1.9, 1.2) on a straight line and in 40 s, while the orientation to change from $45°$ to $0°$, see Fig. 6. External pulse disturbances in the order of magnitude of the maximum joint torques are applied also at the manipulator's joints for 1s (20s-21s).

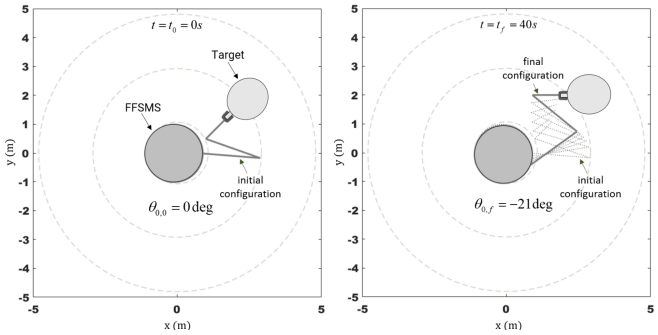

Fig. 6. Motion animation for the desired task.

Fig. 7 shows a comparison between the developed model-based controller with H_∞ and a model-based controller without H_∞, with 2% and 25% uncertainties in S/C and target mass, respectively. Fig. 7(a) and 7(c) compare the end-effector pose (i.e., x_E, y_E, θ_E) tracking errors due to parametric uncertainties only, and to both parametric uncertainties and external pulse disturbance, respectively.

It is evident that the model-based controller with H_∞ results in smaller errors than the one without the H_∞ part, and yet it requires about the same control effort as shown by the applied joint torques in Fig. 7(b). Moreover, Fig. 7(d) shows that the H_∞ controller can attenuate Gaussian noise with zero mean and low standard deviation σ_n. However, at large values of σ_n, the benefit of the H_∞ compensation is reduced. Hence, accurate sensors are essential to yield a benefit from the addition of H_∞ compensation.

To determine to what extent the uncertainties in target and S/C mass may affect system performance, Monte Carlo simulations were carried out. The uncertain parameters range is given by (41) - (42).

The goal was to compute the maximum tracking errors allowing estimates of the sensitivity of the controller to parametric uncertainty. Fig. 8 shows the tracking errors produced by 1000 runs with the same tracking objective as above. It is evident, that in every scenario of the uncertain parameters, the developed controller results in tracking errors, in the order of $10^{-5} m$ and $10^{-3} \deg$ for the end-effector position and orientation respectively, i.e., an order of magnitude smaller than those obtained without H_∞ compensation.

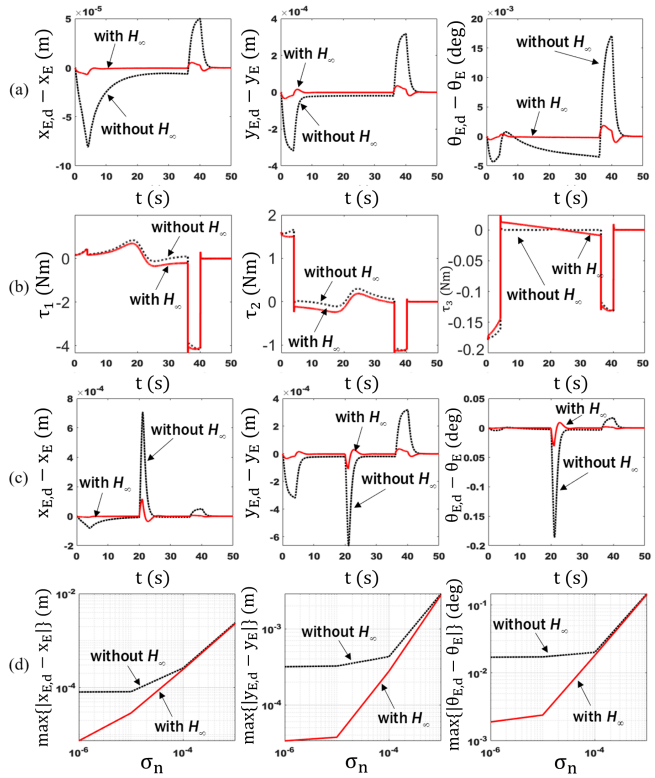

Fig. 7. (a) End-effector tracking errors due to parametric uncertainties, (b) joint torques applied, (c) end-effector trajectory tracking errors due to both parametric uncertainties and external unit-pulse disturbances and (d) noise attenuation properties.

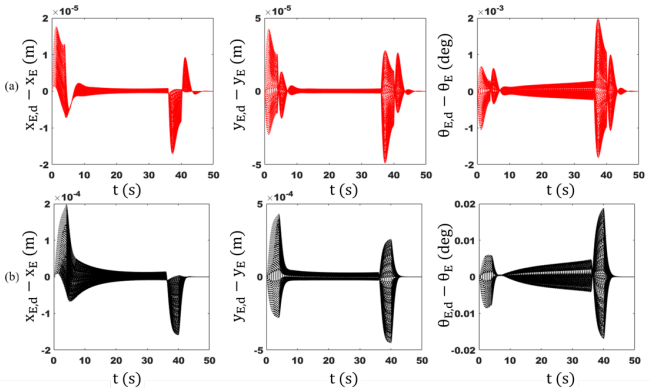

Fig. 8. End-effector tracking errors using (a) the developed controller and (b) a model-based controller without H_∞.

V. Conclusion

A robust controller for the post-capture handling of an unknown object in Cartesian space by an SMS in free-floating mode was developed. The controller consists of two feedback loops. The first is a model-based algorithm, which linearizes the dynamics globally and guarantees specific performance. The second one, is a linear H_∞ law, that adds robustness to the end-effector tracking response. It was shown that the developed controller results in very small tracking errors in the presence of parametric uncertainties and exogenous disturbances, while it attenuates low standard deviation sensor noise. The sensitivity of the developed controller to parametric uncertainties was studied by Monte Carlo simulations and was found that the tracking errors were an order of magnitude smaller than those obtained without H_∞ compensation. The design method applies to spatial systems and was demonstrated by a planar example.

References

[1] Papadopoulos, E., Aghili, F., Ma, O., and Lampariello, R. "Robotic Manipulation and Capture in Space: A Survey," *Frontiers: Robotics & AI - Space Robotics*, 9 July 2021. doi: 10.3389/frobt.2021.686723.

[2] Dubanchet, V., et al., "EROSS Project – Coordinated control architecture of a space robot for capture and servicing operations," *11th Int. ESA Conference on Guidance, Navigation & Control Systems*, June 22 – 25, 2021.

[3] Nanos, K., and Papadopoulos, E. "On the Dynamics and Control of Free-floating Space Manipulator Systems in the Presence of Angular Momentum," *Frontiers: Robotics & AI - Space Robotics,* 4:26, 2017.

[4] Slotine, J.E., Li, W., *Applied Nonlinear Control*, Prentice Hall, 1991.

[5] Ulrich, S., Saenz-Otero, A., Barkana, I., "Passivity-Based Adaptive Control of Robotic Spacecraft for Proximity Operations Under Uncertainties," *Journal of Guidance, Control, and Dynamics*, Vol. 39, No. 6, 2016, pp. 1444-1453.

[6] Papadopoulos, E., "On the Dynamics and Control of Space Manipulators," *Ph.D. Thesis*, Dept. Mech. Eng., MIT, Cambridge, MA, 1990.

[7] Zhou, K., and Doyle, J.C., *Essentials of Robust Control*, Prentice Hall, New Jersey, 1998.

[8] Dastidar, R. G., "On the Advantages and Limitations of Sliding Mode Control for Spacecraft," *AIAA SPACE 2010 Conference & Exposition*, Anaheim, California, August 30 - September 2, 2010.

[9] Safonov, M. G., Chiang, R. Y., and Flashner, H., "H_∞ Robust Control Synthesis for a Large Space Structure," *J. Guidance, Control and Dynamics*, Vol. 14, No. 3, 1991, pp. 513–520.

[10] Charbonnel, C., "H_∞ Controller Design and μ-Analysis: Powerful Tools for Flexible Satellite Attitude Control," *AIAA Guidance, Navigation, Control Conference*, Toronto, Canada, 2010.

[11] Pirat, C., Ankersen, F., Walker, R., and Gass, V., "H_∞ and μ-Synthesis for Nanosatellites Rendezvous and Docking," *IEEE Transactions on Control Systems Technology*, Vol. 28, No. 3, May 2020, pp. 1050 - 1057.

[12] Taveira, T., Siqueira, A., and Terra, M., "Adaptive Nonlinear H_∞ Controllers Applied to a Free-Floating Space Manipulator," *IEEE International Conference on Control Applications*, Munich, Germany, October 4-6, 2006, pp. 1476 - 1481.

[13] Seddaoui, A., and Saaj, C. M., and Eckersley, S., "Adaptive H_∞ Controller for Precise Maneuvering of a Space Robot," *2019 International Conference on Robotics and Automation,* Montreal, Canada, May 20-24, 2019, pp. 4746 - 4752.

[14] Seddaoui, A., and Saaj, C. M., "Combined Nonlinear H_∞ Controller for a Controlled-Floating Space Robot," *Journal of Guidance, Control, and Dynamics,* Vol. 42, No. 8, August 2019, pp. 1878 – 1885.

[15] Seddaoui, A., and Saaj, C. M., "H_∞ Control for a Controlled Floating Robotic Spacecraft," *Int. Symposium Artificial Intelligence, Robotics and Automation in Space*, Madrid, Spain, June 4-6, 2018.

[16] Bueno, J. N. A., Serrantola, W. G., Bezerra, R. A., and Grassi, V., "LQR and H-Infinity Controls of a Free-Floating Space Manipulator with Two Arms," *XIII Latin American Robotics Symposium and IV Brazilian Robotics Symposium*, Pernambuco, Brazil, October 8-12, 2016, pp. 85 – 90.

[17] Nanos, K., and Papadopoulos, E, "Avoiding Dynamic Singularities in Cartesian Motions of Free-floating Manipulators," *IEEE Transactions on Aerospace and Electronic Systems*, Vol. 51, No. 3, July 2015, pp. 51, 2305–2318.

[18] Zhou, K., and Doyle, J.C., *Essentials of Robust Control*, Prentice Hall, New Jersey, 1998.